



# A combined theoretical and *in vitro* modeling approach for predicting the magnetic capture and retention of magnetic nanoparticles *in vivo*

Allan E. David<sup>a</sup>, Adam J. Cole<sup>a</sup>, Beata Chertok<sup>a</sup>, Yoon Shin Park<sup>a</sup>, Victor C. Yang<sup>a,b,\*</sup>

<sup>a</sup> Department of Pharmaceutical Sciences, University of Michigan, Ann Arbor, MI 48109, USA

<sup>b</sup> School of Pharmacy, Tianjin Medical University & Tianjin Key Laboratory for Modern Drug Delivery and High Efficiency, Tianjin 300070, China

## ARTICLE INFO

### Article history:

Received 17 November 2010

Accepted 25 January 2011

Available online 2 February 2011

### Keywords:

Magnetic targeting  
Iron oxide nanoparticle  
Brain tumor  
Drug delivery  
Theoretical modeling

## ABSTRACT

Magnetic nanoparticles (MNP) continue to draw considerable attention as potential diagnostic and therapeutic tools in the fight against cancer. Although many interacting forces present themselves during magnetic targeting of MNP to tumors, most theoretical considerations of this process ignore all except for the magnetic and drag forces. Our validation of a simple *in vitro* model against *in vivo* data, and subsequent reproduction of the *in vitro* results with a theoretical model indicated that these two forces do indeed dominate the magnetic capture of MNP. However, because nanoparticles can be subject to aggregation, and large MNP experience an increased magnetic force, the effects of surface forces on MNP stability cannot be ignored. We accounted for the aggregating surface forces simply by measuring the size of MNP retained from flow by magnetic fields, and utilized this size in the mathematical model. This presumably accounted for all particle–particle interactions, including those between magnetic dipoles. Thus, our “corrected” mathematical model provided a reasonable estimate of not only fractional MNP retention, but also predicted the regions of accumulation in a simulated capillary. Furthermore, the model was also utilized to calculate the effects of MNP size and spatial location, relative to the magnet, on targeting of MNPs to tumors. This combination of an *in vitro* model with a theoretical model could potentially assist with parametric evaluations of magnetic targeting, and enable rapid enhancement and optimization of magnetic targeting methodologies.

© 2011 Elsevier B.V. All rights reserved.

## 1. Introduction

Particulate-based drug carriers, such as nanoparticles, have shown promise in their application to tumor drug targeting [1,2]. In fact, animal studies evaluating drug-loaded nanoparticles have shown up to 60-fold enhanced drug accumulation in tumors, compared to administration of free drug [3]. Among the various nanoparticles studied for therapeutic applications, magnetic nanoparticles (MNP) have received special attention due to their dual-purpose functionality – as both diagnostic (e.g. magnetic resonance imaging – MRI) and therapeutic agents [4].

MNPs generally consist of an iron oxide core (which provides its visibility on MR images and its responsiveness to externally applied magnetic fields) and a polymeric coating that improves particle stability and biocompatibility [5]. As common to many nanoparticulate systems, passive targeting of MNP to tumors can be achieved via the so-called enhanced permeability and retention (EPR) effect [2]. On the other hand, active enhancement of MNP delivery to tumors can be

achieved via tumor targeted ligands (e.g. peptides, antibodies, and small molecules) and/or the application of an external magnetic field [6]. Regardless of method, the goal of any targeting strategy is to improve treatment efficacy while reducing off-target toxicity – in other words, to achieve selectivity. Magnetic targeting is an attractive, non-invasive strategy to selectively accumulate MNPs in tumors. Indeed, in clinical studies, this has been shown to be an effective method in some, but not all, patients [7]. These treatment outcomes could potentially be improved upon with a clearer understanding of the physiological and physical processes involved in magnetic targeting of MNP to tumors.

The general protocol for magnetic targeting involves exposure of the tumor region to an externally applied magnetic field, followed by the administration of MNPs. Subsequent to administration, nanoparticles must first be passively delivered to the lesion by blood flow. Once carried into tumor vasculature, retention of MNP then depends on the interplay between the magnetic and hydrodynamic drag forces, and interactions with the tumor environment [8]. While both *in vitro* and *in vivo* studies have been conducted to elucidate the factors affecting magnetic targeting of MNP, there is still much to understand about the process in order to facilitate clinical translation. In fact, it has been suggested that a lack of understanding of the magnetic targeting process may be hindering its wide application [9]. Therefore, we undertook this study to gain further insight into how

\* Corresponding author at: Prescott Professor of Pharmaceutical Sciences, College of Pharmacy, University of Michigan, Ann Arbor, MI 48109–1065, USA. Tel.: +1 734 764 4273; fax: +1 734 763 9772.

E-mail address: [vcyang@umich.edu](mailto:vcyang@umich.edu) (V.C. Yang).

the forces at play within the tumor and normal tissue environments affect the efficiency of magnetic targeting and the retention of MNPs.

Our previous work has focused on the magnetic targeting of MNP to brain tumors, an indication especially challenging to treat [10]. Work done with glioma bearing rats illustrated that magnetic targeting can indeed increase MNP accumulation in tumors [11] – encouraging further exploration of MNP targeting. Further *in vivo* studies demonstrated that MNP surface chemistry can also be a significant factor that affects tumor accumulation [12,13]. Moreover, a follow-up *in vitro* study, with capillary tubing placed in a magnetic field, showed that abnormal hydrodynamics in brain tumors compared to normal brain (NB), are a likely contributor to the success of magnetic targeting [14]. Indeed, that effort demonstrated that the rate of MNP retention is a function of the carrier fluid's flow velocity (hydrodynamics), which correlated well with *in vivo* data. However, the semi-quantitative nature of that study prevented inspection of the dynamic processes present during magnetic targeting. Here we take a closer examination of the interplay between the magnetic and drag forces under physiological flow conditions present in tumor and NB. By comparison to *in vivo* results, we show that this *in vitro* model provided a surprisingly good approximation of the tumor selectivity of magnetic targeting. We then develop a mathematical model of this particular magnetic targeting system and examine its agreement with our *in vitro* study. Finally, physiological parameters, relevant to glioma bearing rats, are inserted into the model to evaluate how MNP size, distance from the magnet, and magnetic field geometry potentially affect the success of magnetic targeting.

## 2. Material and methods

### 2.1. Materials

Fetal Bovine Serum (FBS) was purchased from Invitrogen and passed through a 0.45 µm filter prior to use. Starch-coated magnetic nanoparticles (FluidMAG-D) were obtained from Chemiceil® GmbH (Berlin, Germany). Polyethylene capillary tubing (PE/3 – 0.058 cm ID) was purchased from Scientific Commodities Inc. (Lake Havasu City, AZ).

### 2.2. *In vitro* simulation of magnetic targeting

Due to the inherent complexity of physiological systems, simplified *in vitro* models are often required to gain insights into the various factors affecting drug delivery processes. For magnetic targeting of MNPs, this is often accomplished by *in vitro* simulations utilizing capillary tubes exposed to a magnetic field gradient, as previously published [14,15]. The *in vitro* retention of MNPs is quantified and used as an estimate of what could be expected *in vivo*. In such manner, the effects of various parameters (e.g. magnet configuration, distance from the magnetic pole, flow velocity, particle size, and particle surface properties) on magnetic targeting efficiency can be studied. However, considering the complexity of magnetic targeting *in vivo*, the simple capillary tubing model would seem unlikely to provide an accurate representation of what occurs in animal models. We therefore first evaluated the accuracy of the capillary tubing model by comparing its retention of MNP, using physiologically relevant blood flows, with previously reported *in vivo* data obtained from tumor-bearing rats.

#### 2.2.1. Configuration of magnet and tubing for *in vitro* studies

Two different magnetic setups were utilized in this study. A “Standard” configuration consisted of a dipole electromagnet (GMW Associates, Model 3470), fitted with poles of 20 mm ID separated by an air gap of 20 mm. The second “Modified” setup was optimized to produce a sharp magnetic flux density, as described previously [12]. Briefly, this consisted of attaching a 9 mm cylindrical neodymium–

iron–boron magnet (AllStar Magnetics Inc., Vancouver, WA) to the beveled-edge of an electromagnet pole. Magnetic field density maps for both configurations were created with spatial measurements of the field strength with a 3-axis Hall Teslameter (Model 7025, GMW Associates, Redwood City, CA).

Capillary tubing was placed at a distance of 7 mm from the center of the magnetic pole, approximating the expected gap between magnet and tumor in targeted glioma-bearing rats [14]. A suspension of MNP in 100% FBS was continuously infused through the tubing with flow rates metered by a syringe pump. MNP concentration was fixed at 74 µg Fe/mL, the initial plasma concentration of starch-MNPs observed after intravenous administration at a dose of 12 mg Fe/kg. Eluent, not retained by the magnet, was collected in 200 µL fractions and the MNP concentration determined by measuring absorbance at 350 nm. Fraction of MNP retained was calculated by mass balance between the measured samples and the original solution. Particle size measurements of both the eluent and retained MNPs were measured using Dynamic Light Scattering (ZetaSizer Nano ZS90, Malvern, Worcestershire, UK).

#### 2.2.2. Determination of physiologically relevant flow velocities for *in vitro* experiments

The capture of MNP was studied under flows corresponding to typical blood flow rates observed in rat normal brain and brain tumors. Physiological parameters reported in literature (see Table 1) were utilized to estimate the linear flow rates, as previously described [14], with the equation,

$$v_L = \frac{PV}{n} \left( \frac{\pi d}{2} \right)^{-2} \left( \frac{3V}{4\pi} \right)^{-2/3} \quad (1)$$

where  $v_L$ , the average linear blood velocity in a single capillary, is a function of the blood perfusion of the tissue ( $P$ ), tissue volume ( $V$ ), microvessel density ( $n$ ), and average capillary diameter ( $d$ ). Using the parameters in Table 1, the estimated linear blood flow rates were  $0.074 \pm 0.051$  cm/s and  $0.31 \pm 0.16$  cm/s for tumor and NB tissues, respectively. Due to limited flow rate settings available on the syringe pump used in the *in vitro* studies, the tumor and NB flows were simulated at values of 0.055 cm/s and 0.365 cm/s, respectively, which are still within one standard deviation of the respective means estimated above.

### 2.3. Theoretical model of magnetic targeting

Upon successful validation of the *in vitro* model, we then simulated the magnetic retention of MNPs in capillary tubing using MATLAB software (MathWorks, Natick, MA). Although blood vessels can take a tortuous path *in vivo* [19], to simplify the model, it was assumed that, as in the capillary tubing experiments, blood vessels in tumor and NB are perfectly straight cylindrical tubes. Due to symmetry, the model was further simplified from three-dimensional to a two-dimensional problem, as shown in Fig. 1. We first ran the model utilizing parameters (e.g. tube diameter and flow velocity) from the *in vitro* capillary tubing study described in Section 2.2. The fraction of MNP retention predicted by the model was then compared to results from the *in vitro* experiments as a means to validate the mathematical model's applicability. It was inferred that, if the *in vitro* simulation was found to provide a reliable approximation of *in vivo* magnetic targeting, and the mathematical model reasonably predicted the *in vitro* data, then the theoretical model could be relied upon to directly provide a description of the *in vivo* magnetic targeting process. If shown to be true, this would greatly assist the parametric evaluation of magnetic targeting, and potentially enable a more rapid optimization for *in vivo* application.

In building the mathematical model, we considered the several forces that act on the MNP when subject to magnetic targeting, including: hydrodynamic drag forces ( $F_d$ ) from the blood stream,

**Table 1**

Parameters used for theoretical estimation of capillary blood flow in tumor and contralateral brain tissue of 9 L glioma bearing rats.

Parameter	Symbol	Units	Tumor	Normal brain	Reference
Blood perfusion	$P$	ml/100 g/min	85.3 ± 26.9	147.7 ± 31.1	[16]
Capillary diameter	$d$	μm	21.0 ± 5.9	7.4 ± 1.4	[17]
Microvessel density	$n$	Vessels/mm <sup>2</sup>	170.9 ± 13.8	534.9 ± 127.2	[18]
Tissue volume	$V$	μL	53 ± 5	53 ± 5	[14]
Calc. linear velocity	$v_L$	cm/s	0.074 ± 0.051	0.31 ± 0.16	[14]

magnetic forces ( $F_m$ ) from the applied magnetic field, gravitational forces, buoyancy forces, and inertial forces. Because they are several orders of magnitude lower than the magnetic force [15], and as it can be assumed that nanoparticles relax instantaneously to the fluid velocity, inertial forces are considered negligible. Gravitational and buoyancy forces are both relatively small for nanoparticles and are also considered negligible [15]. Particles traveling in a velocity gradient experience a lift force perpendicular to the flow direction, moving the particle in the direction of increasing velocity. This force, approximated by calculating the lift velocity of a non-inertia spherical nanoparticle in a laminar flow [20], was found to be several orders of magnitude smaller than the drag and magnetic forces, and was therefore also not considered in the model. Trajectories of nanoparticles can additionally be influenced by Brownian motion and inter-particle forces, which were not accounted for in this model. Thus, two forces remain for consideration – the hydrodynamic force and magnetic force, which act in opposition to each other. The general scheme used for calculation of particle trajectories is based on the method used by Gleich et al. [15], as described below.

### 2.3.1. Hydrodynamic force on a nanoparticle

Hydrodynamic forces on a MNP arise due to differences in particle and fluid velocities. The fluid velocity in the simulated tubing is described by the Navier–Stokes equation. Assuming full laminar flow according to the Hagen–Poiseuille Law, the velocity in a cross-section of a cylindrical tube is derived [15] as the parabolic equation,

$$v_x = \frac{2\bar{v}}{R^2} (R^2 - y^2) \quad (2)$$

where  $v_x$  is the fluid's  $x$ -component linear velocity a distance  $y$  from the tube center line,  $\bar{v}$  is the mean flow velocity, and  $R$  is the tube inner radius. The relative importance of inertial and viscous forces in a flow is provided by the dimensionless Reynolds number,

$$Re = \frac{2\rho\bar{v}R}{\mu} \quad (3)$$

where  $\rho$  and  $\mu$  are the density and dynamic viscosity of the fluid, respectively. For conditions of low Reynolds number ( $Re < 1$ ), the fluid

resistance on a suspended, spherical particle follows Stokes' law in the form,

$$\vec{F}_d = 6\pi\eta r_p (\vec{v}_f - \vec{v}_p) \quad (4)$$

in which  $\eta$  is the fluid viscosity,  $r_p$  is the particle radius, and  $\vec{v}_f$  and  $\vec{v}_p$  the fluid and particle velocities, respectively [21]. The fluid velocity specified here is that at the streamline passing through the center of the particle. From this equation we observe that the particle experiences a drag force only when its velocity magnitude, or direction, differs from that of the fluid. If a particle is resting on the wall of the capillary tube, the drag force on the particle is reduced [21] and approximated as,

$$\vec{F}_{d, wall} = 6\pi\eta r_p \left( \vec{v}_f \frac{4r_p}{R} \right) \left( \frac{25}{16} \right). \quad (5)$$

### 2.3.2. Calculating the magnetic force on a magnetic nanoparticle

The magnetic force on a nanoparticle of magnetic moment  $m$ , acted upon by a magnetic field gradient  $\nabla B$ , can be expressed [5] as

$$\vec{F}_m = (\vec{m} \cdot \nabla) \vec{B}. \quad (6)$$

If it is assumed that the magnetic moments are all aligned with the external magnetic field, the equation of magnetic force on a particle [15] is simplified to

$$\vec{F}_m = m \nabla B. \quad (7)$$

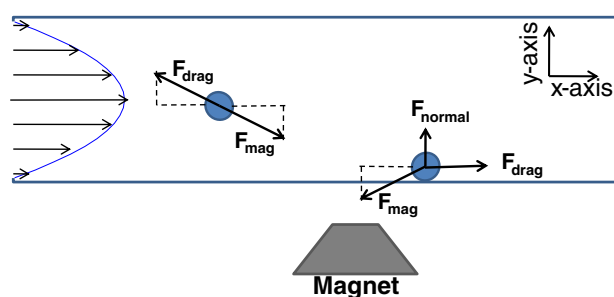
As the Modified magnet used in this work showed significant spatial variation of magnetic flux density, it could not be assumed that magnetic moment of the MNP was saturated at all locations. Therefore the magnetic moment of the particle was measured using a Superconducting Quantum Interference Device (SQUID-MPMS, Quantum Design, San Diego, CA) over a range of applied fields (0–2T), and this integrated into the model.

In order to obtain the magnetic field gradient, we first took measurements of the magnetic field flux density within a region of interest (60 mm × 20 mm grid) perpendicular to the pole face of the test magnet. This data was then uploaded into MATLAB and a surface function created using the *TriScatteredInterp* function. The gradient of this surface was then obtained using the *gradient* function. At any location ( $x, y$ ), the magnetic force vector on a particle is then simply obtained by multiplying the gradient at that location with the appropriately calculated particle magnetic moment.

### 2.3.3. Calculating the trajectories of magnetically targeted MNPs

Applying Newton's Third Law of Motion to the modeled system, the drag force, on a suspended particle, is the equal and opposite reaction to the magnetic force. Therefore, the force balance (assuming steady-state) is simply,

$$-\vec{F}_d = \vec{F}_m \quad (8)$$

**Fig. 1.** General scheme for magnetic targeting of iron oxide nanoparticles to tumors.

$$-6\pi\eta r_p(\vec{v}_f - \vec{v}_p) = m\nabla B. \quad (9)$$

The particle velocity vector then, obtained by rearranging Eq. (9), is

$$\vec{v}_p = \frac{m}{6\pi\eta r_p} \nabla B + \vec{v}_f. \quad (10)$$

In the mathematical model, a tubing segment (60 mm length) was placed on a plane parallel to, and 7 mm above, the magnet pole face, and with the tubing mid-point aligned to the pole center. MNP particles ( $n=21$ ) were located at the inlet of the tubing, equally spaced across the tube diameter, and with initial velocities determined by Eq. (2). Iterative calculations were conducted to determine the particle velocity and positions with,

$$\vec{v}_{i,t+1} = \frac{m}{6\pi\eta r_p} \nabla B + \vec{v}_f \quad (11)$$

$$(x,y)_{i,t+1} = (x,y)_{i,t} + \frac{(\vec{v}_{i,t} + \vec{v}_{i,t+1})}{2} \Delta t \quad (12)$$

where  $i$  represents the  $i$ th particle,  $t$  is the iteration number, and  $\Delta t$  is the time-step. Iterations were continued for each particle until the particle either reached the tubing wall or exited the capillary segment. The fraction of particles retained ( $R$ ) by the magnetic force was then calculated as the ratio,

$$R = \frac{N_w}{N_w + N_e} \quad (13)$$

where  $N_w$  is the number of particles reaching the wall, and  $N_e$  is the number exiting the tubing;  $N_w + N_e = 21$  for each simulation run.

#### 2.3.4. Determining regions of MNP accumulation within the capillary tubes

Particles are only captured from flow when: 1) they are in contact with the capillary wall; and 2) they have a zero velocity. And since particles at rest in a moving fluid experience a drag force, there must be a component of the magnetic force of sufficient strength to overcome the drag in order to retain a particle. We therefore surmised that the probability of particle retention at any point in the capillary is proportional to the ratio of the magnetic and drag forces, calculated for particles resting on a wall (i.e.  $\vec{F}_m / \vec{F}_{d, wall}$ ).

Accumulation of MNP during magnetic targeting results in a reduction of the cross-sectional area of the flow channel (i.e. MNP accumulation plugs a section of the tubing), and the resulting change in fluid velocity must be accounted for in calculating the drag forces. This was accomplished by assuming that for every point within the tubing of radius  $R$  (where  $r \leq R$ ) and at radial distance  $dx$  away from the capillary wall closest to the magnet, the effective diameter of the tube at that location is  $2R - dx$  and not  $2R$ . This results in a mean fluid velocity increase proportional to the change in tubing cross-sectional area, or

$$v_r = \bar{v} \left( \frac{R^2}{\left( \frac{2R-dx}{2} \right)^2} \right). \quad (14)$$

This increased velocity and the reduced effective capillary radius were utilized in calculating the flow velocity profile according to Eq. (2), and taken into account when estimating the  $\vec{F}_m / \vec{F}_{d, wall}$  ratio. It is expected that a plot of this ratio, across the entire tubing volume,

would provide some estimation of the equilibrium accumulation of MNPs within the capillary tube.

### 3. Results

#### 3.1. In vitro simulation of magnetic targeting

Magnetic retention of MNPs was monitored with two different targeting magnet configurations. These two magnet configurations, labeled Standard and Modified, enabled us to evaluate the effects of magnetic flux density geometry on the capture of MNP. The Standard setup displayed high magnetic flux densities of approximately 400 mT at its peak, see Fig. 2A, and minimum of about 200 mT at an  $x$ -axis distance of 30 mm from pole center. However, as seen in Fig. 2B, the magnetic flux density of the Modified setup ranges from approximately 250 mT, at the pole center, to 20 mT when measured 30 mm away.

Photographic images of MNP retention in the capillary tubing, positioned within the Standard or Modified setups, at tumor and NB flows are shown in Fig. 3. With the Standard magnet and NB flow, particles were seen to accumulate in low lying “dunes” running across the entire pole face of the magnet, and slightly increased accumulation downstream from center.

At their peak, the accumulated nanoparticles appear to occupy approximately 50% of the tube diameter. When fed with MNP solution at the slower tumor flow rate, a large plug of MNP, blocking about 75% of the tube diameter, is observed at the upstream edge of the magnetic pole. Small amounts of particles are seen across the pole face, and a small bump of increased accumulation at the downstream edge of the pole. Conversely, accumulation with the Modified setup is centered on the pole face for both NB and tumor flow rates, with far greater retention observed at the slower flow rate. Greater than 75% of the tubing is blocked at the tumor flow rate, compared to <50% under NB conditions. Indeed, some large, unretained MNP aggregates can be observed moving downstream from the magnet at the NB flow velocity in the Modified setup.

Quantitative analysis, see Fig. 4A, showed that  $15.9 \pm 2.6\%$  and  $85.4 \pm 0.6\%$  of MNP are retained by the Standard magnet at the NB and tumor flow velocities, respectively. The Modified magnet yielded NB and tumor flow accumulations of  $5.0 \pm 2.9\%$  and  $81.9 \pm 1.4\%$ , respectively. All measurements were found to be statistically different ( $p < 0.01$ ) from each other by two-tailed, unpaired  $t$ -test.

Dynamic Light Scattering measurement showed hydrodynamic sizes ranging between 600 and 800 nm for particles retained by magnetic targeting, with all magnet configuration and flow velocity combinations, see Fig. 4B–C. However, MNP in the NB outflow, eluting downstream of the magnet, were measured with a mean size of 200 nm. While the tumor outflow showed the presence of larger aggregates, with mean sizes of 700 and 400 nm for the Standard and Modified magnets, respectively, it should be kept in mind that the fraction of particles in the outflow at the slower, tumor flow rates is relatively small. The mean size of MNPs in FBS and not exposed to magnetic fields was found to be approximately 200 nm (not shown).

#### 3.2. Theoretical modeling of MNP capture

For validation of the theoretical model, runs were conducted with MNP size set to 700 nm based on the particle sizes measured for retained MNP in the *in vitro* study. Representative trajectories for magnetic nanoparticles moving past the magnet are shown in Fig. 5A. Each panel shows a full cross-section of the capillary tubing (60 mm length  $\times$  0.58 mm diameter) with streamlines, each indicating the calculated path of a MNP. From these trajectories, the fraction of particles retained by the magnet was determined as the ratio of particles reaching the capillary wall to the total number of particles



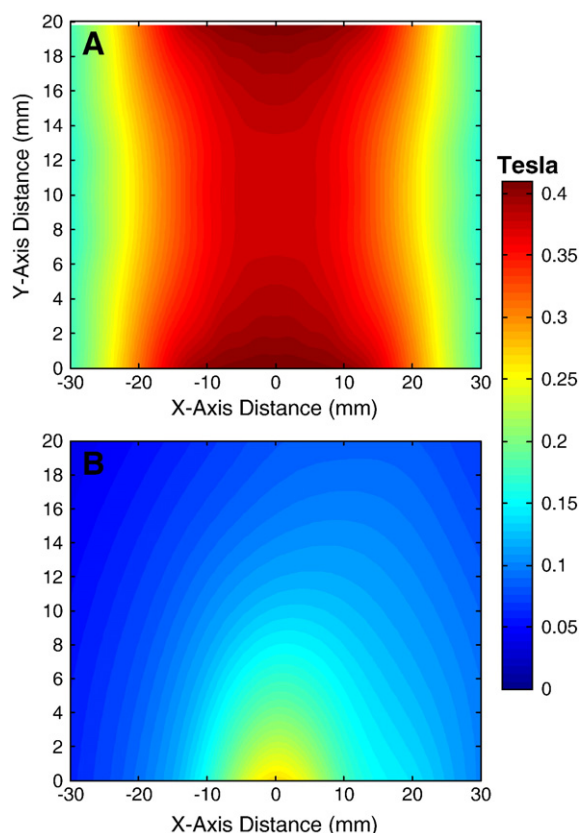


**Fig. 2.** Magnetic flux density maps, perpendicular to plane of the magnet pole face, for the Standard (A) dipole electromagnet and the Modified (B) focused magnet. Capillary tubing was placed parallel to the x-axis at specified y-axis distance. MNP solution flow was from left to right, with respect to the maps.

( $n = 21$ ). The percent MNP capture predicted by the theoretical model is given in Table 2.

Since MNP capture occurs only where the magnetic force is of sufficient strength to counteract the drag force, we then explored the ratio of  $F_m/F_d$ , wall as a predictor of localization of MNP accumulation. Fig. 5B shows the ratio of the magnetic and drag forces at each point along the capillary tube, with the assumption that the regions below the calculated point have been filled with accumulated MNP. Accumulation of MNP narrows the local flow space, which results in an increase of fluid velocity and the associated hydrodynamic drag force. The large panels in Fig. 5B show the  $F_m/F_d$  wall ratio with respect to the y-directional magnetic force, perpendicular to the magnet pole face, while the insets show it with respect to the x-directional magnetic force; the computed axial (x-directional) drag

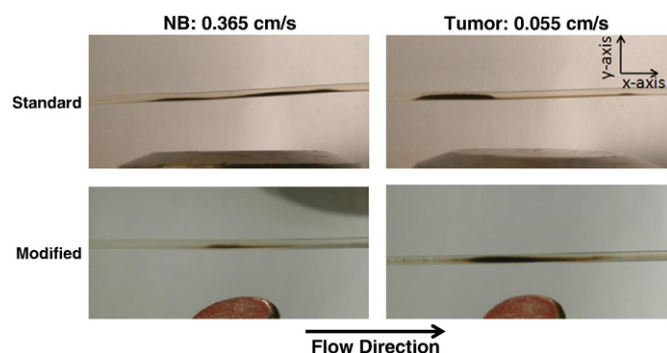


**Fig. 3.** Simulation of magnetic capture of MNP utilizing the Standard and Modified dipole magnets configurations, with mean flow velocities corresponding to normal brain (NB) and tumor values estimated from literature.

force is utilized in all cases. The importance of these two (x- and y-directional) ratios is discussed later. As seen by the maps, the ratio of the forces was much greater at the lower tumor flow velocities compared to NB flow; indicating a greater net retaining force at the lower flows. Additionally, the Standard setup seemed to provide a much broader region for MNP retention, compared to the narrower retention area of the Modified magnet configuration.

### 3.3. Calculation of MNP trajectories in normal brain and tumor capillaries

Since the theoretical model described above approximated the *in vitro* experiments reasonably well, we then simulated the trajectories of MNP in tubing with sizes equivalent to tumor and NB capillary diameters (parameters specified in Table 1), and used the corresponding flow velocities calculated in Section 2.2.2. First, we maintained the capillary at the original y-position (7 mm above the magnetic pole), varied the MNP size (10–800 nm diameters), and determined the fraction of MNP drawn in contact with the capillary wall. Because the outcomes were similar with both the Standard and Modified magnet configurations, only simulation data for the Standard magnet are shown (see Fig. 6A). Results showed that for particles <50 nm in diameter, there is not much difference between the tumor and NB capillaries in the number of particles contacting the vessel wall. However, as the particle size increases above 50 nm, a greater fraction of MNP contact the wall in the tumor vessel compared to NB, with a maximum difference observed with a MNP diameter of

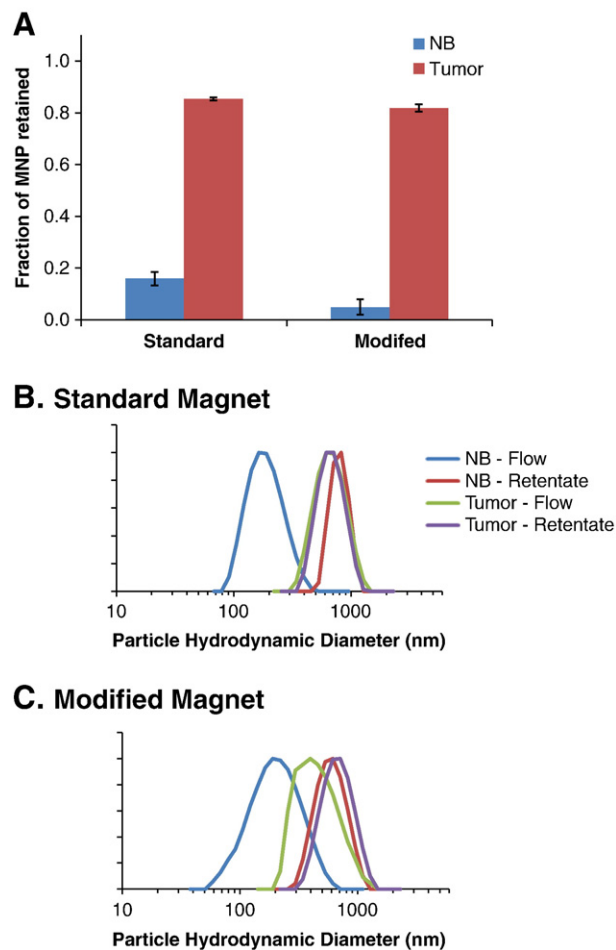


**Fig. 4.** (A) Fraction of D-MNP in tubing outflow with different magnet configurations, and at NB and tumor flow rates. (B) and (C) show particle size analysis of both outflow and retentate, at the two flow velocities, for the standard and modified magnet configurations, respectively.

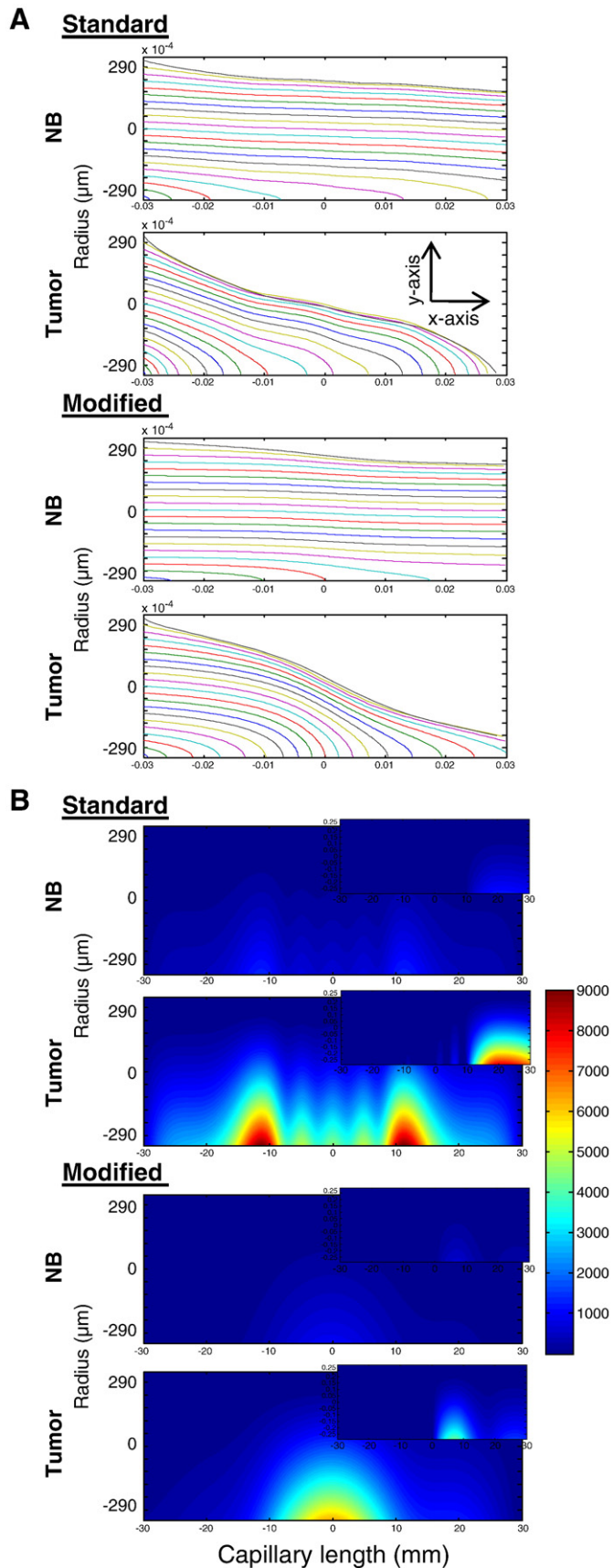


**Fig. 5.** (A) Trajectories of D-MNP particles and (B) the ratio of their  $F_m/F_d$  across the capillary tube, at normal brain and tumor flow rates, for both the standard and modified magnet configurations. Large panels show the ratio with respect to y-directional magnetic force, while the insets show it with respect to the x-direction force.

about 150 nm. Once the MNP size reaches 200 nm and above (data not shown), 100% of the MNPs in both the tumor and NB vessels are predicted to contact the capillary wall. It should be noted that the physiologically relevant capillary diameters used here are much smaller than the 580 μm tubing used in the *in vitro* studies. Therefore, any MNP would have to transit a greatly reduced distance prior to wall contact, as compared to the previous *in vitro* situation.

Since magnetic field gradients drop sharply with distance from the magnet, MNP retention would also be expected to depend on tissue spatial coordinates. Taking the 200 nm MNP as an example, we then evaluated the effect of capillary distance from the magnet, along the y-axis, on the fraction of MNPs contacting the vessel surface. With the Standard magnet (data not shown), no difference between the tumor and NB capillaries was observed, with all particles reaching the surface at all distances (except for when the capillary was placed exactly between the two poles where the gradient is negligible, and all particles pass through the capillary without touching the wall surface). However, a distinct difference was observed in the tumor and NB vessels with the Modified magnet, as seen in Fig. 6B. With 200 nm MNP and NB conditions, the fraction of particles reaching the wall drops from 100% at a distance of 1 mm to approximately 35% at a 30 mm distance. However, under tumor conditions, MNP are completely deflected to the wall at distances up to 7 mm, from where it also begins to drop-off to about 40% of MNP at 30 mm away. The fraction of MNP reaching the capillary wall in the tumor vessel was always greater than that for a NB vessel placed at the same distance from the magnet, with a maximum difference occurring at approximately 7 mm from the Modified magnet.

Since contact between particle and wall is not sufficient for retention, we then examined the ratios of magnetic and drag forces, as previously described, within the physiologically-relevant NB and tumor capillaries. Fig. 6C shows the maximum ratio of the magnetic force (perpendicular to bulk flow) to the axial drag force ( $F_{m,y}/F_d$ , wall) predicted by the model under NB and tumor physiological conditions; area maps closely resembled those in Fig. 5B with appropriate adjustment of the color bar and are therefore not shown. The peak ratio was below unity in NB conditions for both magnet configurations at 0.28 and 0.11, respectively, for Standard and Modified setups. With tumor parameters, the magnetic-drag force ratio was increased by approximately 33-fold, compared to corresponding NB, to 9.3 and 3.8 for the Standard and Modified configurations, respectively.

**4. Discussion**

Magnetic targeting of MNPs to tumors is a complex process affected by many factors, including a number of body and surface forces. Many of these factors, however, are often excluded from models to simplify the system for theoretical considerations. With nanoparticulate systems, it is often found that body forces (e.g. gravity and buoyancy) can be negligible due to the minute particle volume. Surface forces, on the other hand, can be substantial due to the increased surface/volume ratio of nanoparticles [22]. However, many theoretical treatments of the magnetic targeting of MNP make the

**Table 2**  
Comparison of MNP retention predicted by the theoretical model to the *in vitro* results.

Flow velocity	Percent of MNP retained	
	Theoretical	Experimental
Standard magnet		
Normal brain	28.6	15.9 ± 2.6
Tumor	95.2	85.4 ± 0.6
Modified magnet		
Normal brain	14.3	5.0 ± 2.9
Tumor	76.2	81.9 ± 1.4

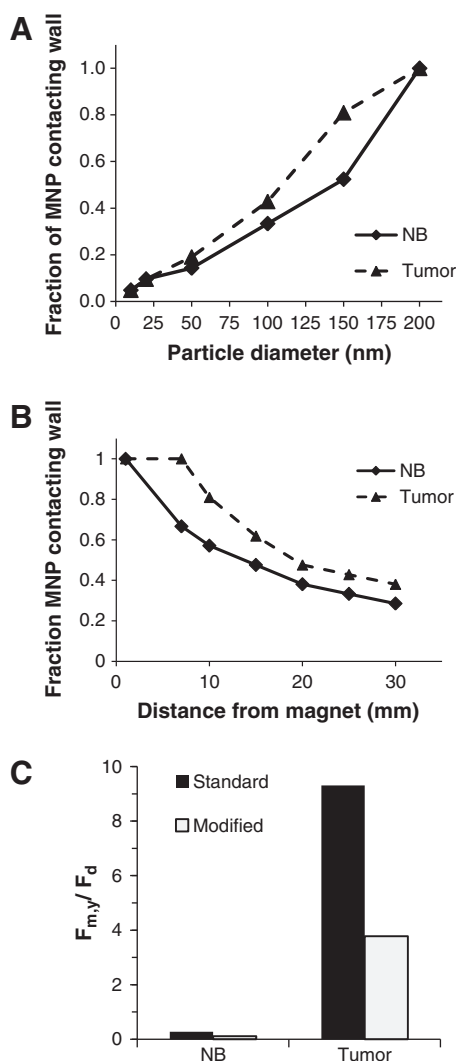


**Fig. 6.** Under physiological conditions for NB and tumor, (A) a comparison of fraction of MNP contacting capillary wall when targeted with the Standard magnet; (B) effect of distance from “Modified” magnetic pole on capture of 200 nm diameter MNP; and (C) maximal  $F_{m,y}/F_d$  across the capillary tube for both the Standard and Modified magnet configurations.

assumption that consideration of hydrodynamic drag and magnetic forces alone is sufficient to approximate particle behavior [15,23]. Our goal in this study was to gain insight into effects of the interplay between the physiological environment and the forces acting upon MNP during magnetic targeting.

The Standard, dipole electromagnet, exhibited a fairly uniform magnetic field between the two pole faces, and slowly diminishing fields moving away along the  $x$ -axis. The ratio of particles retained by the Standard magnet under tumor versus NB conditions, 5.7-fold difference, is remarkably close to the 9.5-fold difference in MNP concentrations previously measured *in vivo*, in tumor ( $29.8 \pm 7.9$  nmol Fe/g tissue) and contra-lateral normal brains ( $3.1 \pm 2.1$  nmol Fe/g tissue) following magnetic targeting of MNP in glioma bearing rats [11]. On the other hand, the Modified configuration, which was developed for tumor specific delivery of cationic MNPs [12,24], displayed a relatively focused field over a region about 10 mm high and 20 mm wide. This focusing of magnetic field gradient provided a 16.4-fold greater MNP retention under tumor conditions ( $81.9 \pm 1.4\%$ ) compared to the NB ( $5.0 \pm 2.9\%$ ). This result also agreed reasonably well with *in vivo* studies, conducted with the focused magnet and glioma bearing rats, which showed an approximately 9.3-fold greater

accumulation of MNP in tumors ( $42.7 \pm 19.5$  nmol Fe/g tissue) compared to normal brain ( $4.6 \pm 1.1$  nmol Fe/g tissue) [12]. The consistency of the *in vitro* results with *in vivo* data is surprising considering the simplicity of the capillary tubing model, and would seem to indicate that consideration of hydrodynamic and magnetic forces is sufficient for predicting the selectivity of magnetic targeting of MNP to tumors.

However, examination of particle size data showed that particles retained by magnetic targeting, with both magnet configurations and under all flow conditions, consisted of large aggregates of MNP. While the magnetic force is a body force, the aggregation of particles depends on surface forces [22], which apparently is an important, and poorly explored, component of magnetic targeting. When the same experiment was conducted with identical MNP suspended in milliQ- $H_2O$  instead of FBS, no obvious retention was observed (unpublished data), and MNP diameter was measured at approximately 140 nm in the outflow, indicating no aggregation. It is probable that suspension of MNP in FBS, as used in this study and which has greater physiological relevance than water or buffers, results in the surface coating of particles with destabilizing, biological components [25]. Although the particles appeared to maintain some short-term stability in FBS, aggregation was apparent soon after its exposure to magnetic fields, likely due to strong particle–particle interactions.

The dramatic differences obtained with the water- and FBS-suspended MNP illustrate the importance of surface interactions in MNP targeting. While the results with FBS correlate well with *in vivo* data, the water-based studies suggested that MNP accumulation should not occur at either the NB or tumor flow conditions. In fact, others have concluded that magnet targeting of MNP is not feasible from purely theoretical estimates [15], and this may be due to a failure to consider the aggregating potential of MNP *in vivo*. Simply suspending the MNP in FBS, or other appropriate medium, and measuring particle size for inclusion in the theoretical models is also not sufficient. The size of MNP, used in this study, in FBS and not exposed to magnetic fields was measured at approximately 200 nm diameter. However, when this size is used in the theoretical model, only minimal MNP deflection to the wall was observed under tumor flows and none under NB flow – in disagreement with both *in vitro* and *in vivo* data. It is only when the appropriate size of MNP, in FBS and exposed to the magnetic field – capturing the interplay between surface and body forces – is utilized that the theoretical model agreed with the *in vitro* and *in vivo* experimental results.

Using the model, we also took a closer look at the magnetic and drag force balance necessary for retention of MNP. For an MNP resting on the capillary wall, as shown in Fig. 1, it would be expected that the most important magnetic force component for retention would be that in the direction (along the  $x$ -axis) opposite to fluid flow. However, when the capillary accumulation images in Fig. 3 are compared to the  $F_m/F_d$  wall panels in Fig. 5B, we see that the pattern of accumulation more closely resembles the hot spots present in the  $y$ -directional field maps (large panels) rather than, as expected, the  $x$ -directional maps (insets). From the capillary tubing study, we observed that the very initial accumulation in fact did correspond closely with regions predicted by the  $x$ -direction maps. However, as MNP were continuously introduced to the system, the pattern of retained MNPs then quickly started to resemble that predicted by the  $y$ -field maps. A possible explanation is the presence of frictional forces along the tubing surface, which were not included in the model and may be significant due to the relatively high  $y$ -directional magnetic field gradient. Another possibility is that once a particle is captured on the inner surface of the capillary tube, the laminar fluid flow lines must either flow up and over the particle, or dislodge the particle to continue on a straight path. If the flow does in fact trend upward, carrying MNPs in the same direction, then the magnetic force component opposing the particle flow would in fact be the  $y$ -directional force. While the truth may be one or a combination of



these possibilities, comparison of the  $y$ -field ratio maps to the *in vitro* results seem to suggest this as a good predictor of not only regions of MNP accumulation, but also the extent of capillary blockage by the retained MNP – which could be important in monitoring the potential for embolism by targeted MNP.

With validation that the theoretical model performed reasonably well in predicting both the fractional retention and accumulating regions of MNP during magnetic targeting, we then explored actual physiological conditions for tumor and NB capillaries (see Table 1) with the model. From the results in Fig. 6, it would then seem that judicious selection of MNP size and variation of distance from the magnetic source could both be potentially utilized to modulate the efficiency and selectivity of MNP capture of tumor versus NB. While this is probably true in some situations, the overriding importance of hydrodynamics becomes apparent when considering Fig. 6C, which plots the peak  $y$ -directional  $F_m/F_d$ , wall calculated by the model for both tumor and NB vessels. We see that in the tumor capillary, the  $y$ -field magnetic force is approximately 4- and 9-fold greater than the drag force with the Modified and Standard magnets, respectively – suggesting that 200 nm MNP would accumulate within the tumor vessel. Conversely, the magnetic force is only a fraction of the potential drag force in NB capillaries with both magnet configurations; therefore, accumulation of 200 nm MNP is unlikely to occur within the NB vessel, regardless of the fraction of particles reaching the wall. This combination of retention in tumors with no accumulation in NB provides a vital means for selective delivery of MNP to tumor lesions. The greater retaining force ratio of the Standard magnet, compared to the Modified, would seem to indicate that the dipole magnet would provide for greater accumulation in tumor lesions while not yielding on selectivity. However, the theoretical model did predict accumulation within NB vessels when particle size is on the scale of a few micrometers. In the event that MNP grow to such large aggregates, which could be expected with MNPs unstable in physiological fluids, wide-spread accumulation would be observed with the Standard setup. On the other hand, because the applied magnetic force, and therefore the MNP magnetic moment, is much lower with the Modified magnet, only small regions of accumulation would be expected with the focused setup. In fact, *in vivo* studies with highly cationic MNPs found to be unstable in serum, displayed this exact phenomena [24]. Additionally, this theoretical model does not account for interactions with the capillary surface *in vivo* which could be substantial, and potentially enhanced by  $y$ -directional magnetic forces, depending on surface properties of the MNP.

## 5. Conclusions

In conclusion, although the *in vitro* tubing flow model used to simulate magnetic targeting of MNP in animals is rather simplistic compared to physiological conditions, our study has shown its surprising ability to predict the selectivity of MNP capture in tumor versus NB. In order to better understand the process of magnetic retention of MNP, we then developed a theoretical model and confirmed its validity against the previous *in vitro* results. Although the mathematical model itself only accounted for the magnetic force on an MNP, from the applied magnetic field, and drag forces from the flowing fluid, surface forces and particle-particle attraction forces were accounted for by utilizing particle size data from the *in vitro* study. This proved to be important for obtaining an accurate prediction of the *in vitro* retention of MNPs. Once validated, the mathematical model provided fairly accurate estimations of the regions of MNP retention in the *in vitro* study and the extent of accumulation in the capillary tubes. Overall, the theoretical model, combined with simple *in vitro* experiments, show promise as a tool for enhancing and optimizing the magnetic targeting of MNP to tumors.

## Acknowledgements

This work was supported in part by the National Institutes of Health (NIH) R01 Grants CA114612 and NS066945, and a Hartwell Foundation Biomedical Research Award. This work was also partially sponsored by Grant R31-2008-000-10103-01 from the World Class University (WCU) project of South Korea. Victor C. Yang is currently a participating faculty member in the Department of Molecular Medicine and Biopharmaceutical Sciences, Seoul National University, South Korea. In addition, the project was partially sponsored by the National Basic Research Program of China (973 Program) 2007CB935800. Adam Cole is the recipient of a NIH Pharmacological Sciences and Bio-related Chemistry Training Grant (GM007767 from NIGMS), a University of Michigan Rackham Pre-Doctoral Fellowship, and is currently an American Foundation for Pharmaceutical Education (AFPE) Pre-Doctoral Fellow. Beata Chertok was a recipient of the University of Michigan Rackham Graduate School Pre-doctoral Fellowship.

## References

- [1] S.C.J. Steiniger, J. Kreuter, A.S. Khalansky, I.N. Skidan, A.I. Bobruskin, Z.S. Smirnova, S.E. Severin, R. Uhl, M. Kock, K.D. Geiger, S.E. Gelperina, Chemotherapy of glioblastoma in rats using doxorubicin-loaded nanoparticles, *Int. J. Cancer* 109 (5) (2004) 759–767.
- [2] H. Maeda, J. Wu, T. Sawa, Y. Matsumura, K. Hori, Tumor vascular permeability and the EPR effect in macromolecular therapeutics: a review, *J. Control. Release* 65 (1–2) (2000) 271–284.
- [3] A.E. Gulyaev, S.E. Gelperina, I.N. Skidan, A.S. Antropov, G.Y. Kivman, J. Kreuter, Significant transport of doxorubicin into the brain with polysorbate 80-coated nanoparticles, *Pharm. Res.* 16 (10) (1999) 1564–1569.
- [4] J.R. McCarthy, R. Weissleder, Multifunctional magnetic nanoparticles for targeted imaging and therapy, *Adv. Drug Deliv. Rev.* 60 (11) (2008) 1241–1251.
- [5] Q.A. Pankhurst, et al., Applications of magnetic nanoparticles in biomedicine, *J. Phys. D Appl. Phys.* 36 (13) (2003) R167.
- [6] J. Dobson, Magnetic nanoparticles for drug delivery, *Drug Dev. Res.* 67 (1) (2006) 55–60.
- [7] A.S. Lubbe, C. Bergemann, H. Riess, F. Schriever, P. Reichardt, K. Possinger, M. Matthias, B. Dorken, F. Herrmann, R. Gurtler, P. Hohenberger, N. Haas, R. Sohr, B. Sander, A.-J. Lemke, D. Ohlendorf, W. Huhnt, D. Huhn, Clinical experiences with magnetic drug targeting: a phase I study with 4'-epidoxorubicin in 14 patients with advanced solid tumors, *Cancer Res.* 56 (20) (1996) 4686–4693.
- [8] P.A. Voltairas, D.I. Fotiadis, L.K. Michalis, Hydrodynamics of magnetic drug targeting, *J. Biomech.* 35 (6) (2002) 813–821.
- [9] H.D. Liu, W. Xu, S.G. Wang, Z.J. Ke, Hydrodynamic modeling of ferrofluid flow in magnetic targeting drug delivery, *Appl. Math. Mech.-Engl. Ed.* 29 (10) (2008) 1341–1349.
- [10] L. Arko, I. Katsyv, G.E. Park, W.P. Luan, J.K. Park, Experimental approaches for the treatment of malignant gliomas, *Pharmacol. Ther.* 128 (1) (2010) 1–36.
- [11] B. Chertok, B.A. Moffat, A.E. David, F. Yu, C. Bergemann, B.D. Ross, V.C. Yang, Iron oxide nanoparticles as a drug delivery vehicle for MRI monitored magnetic targeting of brain tumors, *Biomaterials* 29 (4) (2008) 487–496.
- [12] B. Chertok, A.E. David, V.C. Yang, Polyethyleneimine-modified iron oxide nanoparticles for brain tumor drug delivery using magnetic targeting and intracarotid administration, *Biomaterials* 31 (24) (2010) 6317–6324.
- [13] B. Chertok, A.E. David, B.A. Moffat, V.C. Yang, Substantiating *in vivo* magnetic brain tumor targeting of cationic iron oxide nanocarriers via adsorptive surface masking, *Biomaterials* 30 (35) (2009) 6780–6787.
- [14] B. Chertok, A.E. David, Y. Huang, V.C. Yang, Glioma selectivity of magnetically targeted nanoparticles: a role of abnormal tumor hydrodynamics, *J. Control. Release* 122 (3) (2007) 315–323.
- [15] B. Gleich, N. Hellwig, H. Bridell, R. Jurgons, C. Seliger, C. Alexiou, B. Wolf, T. Weyh, Design and evaluation of magnetic fields for nanoparticle drug targeting in cancer, *IEEE Trans. Nanotechnol.* 6 (2) (2007) 164–170.
- [16] A.C. Silva, S.G. Kim, M. Garwood, Imaging blood flow in brain tumors using arterial spin labeling, *Magn. Reson. Med.* 44 (2) (2000) 169–173.
- [17] A.P. Pathak, K.M. Schmainda, B.D. Ward, J. Linderman, K.J. Rebro, A.S. Greene, MR-derived cerebral blood volume maps: issues regarding histological validation and assessment of tumor angiogenesis, *Magn. Reson. Med.* 46 (4) (2001) 735–747.
- [18] O. Arosarena, C. Guerin, H. Brem, J. Laterra, Endothelial differentiation in intracerebral and subcutaneous experimental gliomas, *Brain Res.* 640 (1–2) (1994) 98–104.
- [19] P. Vajkoczy, M.D. Menger, Vascular microenvironment in gliomas, *J. Neurooncol.* 50 (1–2) (2000) 99–108.
- [20] R.W. Mei, J.F. Klausner, Shear lift force on spherical bubbles, *Int. J. Heat Fluid Flow* 15 (1) (1994) 62–65.
- [21] C.F. Driscoll, R.M. Morris, A.E. Senyei, K.J. Widder, G.S. Heller, Magnetic targeting of microspheres in blood flow, *Microvasc. Res.* 27 (3) (1984) 353–369.



- [22] W. Peukert, H.-C. Schwarzer, F. Stenger, Control of aggregation in production and handling of nanoparticles, *Chem. Eng. Process.* 44 (2) (2005) 245–252.
- [23] C. Alexiou, D. Diehl, P. Henninger, H. Iro, R. Rockelein, W. Schmidt, H. Weber, A high field gradient magnet for magnetic drug targeting, *IEEE Trans. Appl. Supercond.* 16 (2) (2006) 1527–1530.
- [24] B. Chertok, A.E. David, V.C. Yang, Magnetically-Enabled and MR-Monitored Selective Brain Tumor Protein Delivery in Rats. *Nat. Nanotechnol.* (2010 (In submission)).
- [25] M.S. Ehrenberg, A.E. Friedman, J.N. Finkelstein, G. Oberdörster, J.L. McGrath, The influence of protein adsorption on nanoparticle association with cultured endothelial cells, *Biomaterials* 30 (4) (2009) 603–610.